SCIENCE CHINA
Technological Sciences

Special Topic: Neurodynamics
• Article •

May 2014 Vol.57 No.5: 893–904
doi: 10.1007/s11431-014-5536-y

Stability switches and Bogdanov-Takens bifurcation in an inertial two-neuron coupling system with multiple delays

SONG ZiGen[1] & XU Jian[2*]

[1] *College of Information Technology, Shanghai Ocean University, Shanghai 201306, China;*
[2] *School of Aerospace Engineering and Applied Mechanics, Tongji University, Shanghai 200092, China*

Received March 6, 2014; accepted April 1, 2014; published online April 18, 2014

In this paper, we investigate an inertial two-neural coupling system with multiple delays. We analyze the number of equilibrium points and demonstrate the corresponding pitchfork bifurcation. Results show that the system has a unique equilibrium as well as three equilibria for different values of coupling weights. The local asymptotic stability of the equilibrium point is studied using the corresponding characteristic equation. We find that multiple delays can induce the system to exhibit stable switching between the resting state and periodic motion. Stability regions with delay-dependence are exhibited in the parameter plane of the time delays employing the Hopf bifurcation curves. To obtain the global perspective of the system dynamics, stability and periodic activity involving multiple equilibria are investigated by analyzing the intersection points of the pitchfork and Hopf bifurcation curves, called the Bogdanov-Takens (BT) bifurcation. The homoclinic bifurcation and the fold bifurcation of limit cycle are obtained using the BT theoretical results of the third-order normal form. Finally, numerical simulations are provided to support the theoretical analyses.

inertial two-neuron system, multiple delays, stability switches, Bogdanov-Takens bifurcation, multiple stability

Citation: Song Z G, Xu J. Stability switches and Bogdanov-Takens bifurcation in an inertial two-neuron coupling system with multiple delays. Sci China Tech Sci, 2014, 57: 893–904, doi: 10.1007/s11431-014-5536-y

1 Introduction

The dynamic analysis of neural systems has drawn significant attention since Hopfield established a simplified network model [1]. However, as the number of neurons in a Hopfield network increases, the analysis of such a system tends to become intractable. To solve this difficulty, Schieve et al. [2] proposed the idea of an effective neuron to simplify the study of large Hopfield network systems. The dynamics of a single effective neuron or a few neuronal systems [3,4] have been analyzed in detail in the theory of nonlinear dynamics.

In the inertial neuron model, inertia is introduced from the biological viewpoint. For example, a hair cell-membrane in semicircular canals can be described by an equivalent circuit containing inductances [5,6]. Further, squid axons are modelled to include the phenomenological inductance [7]. Therefore, neural networks with an inertial term can characterize biological neural dynamics well. Babcock and Westervelt [8] combined the inertial term into a single effective neuron, where the delay was introduced using the neuron self-feedback. The neural output was connected to its input through an RLC circuit. Chaotic behavior has also been explored in a two-neuron coupling system. Wheeler and Schieve [9] discuss equilibrium stability and chaos in a two-neuron model with one/two inertial terms. Tain et al. [10,11] included an inertial term into neuronal models for chaotic memorial searching.

In real neural network systems, time delays are an im-

*Corresponding author (email: xujian@tongji.edu.cn)

portant effect of transmission dynamic behavior because of transmitter releasing dynamics and transmembrane resistance [12,13]. The dynamic analysis of an inertial neuron network with delayed coupling has also been a subject of extensive research. Liao's research group systematically considered a single delayed neural model with an inertial term. The Hopf bifurcation [14], chaotic behavior [15], and stability of bifurcating periodic solution [16] were investigated in detail using the normal form theory, non-monotonic activation function, and mean value theorem. Two inertial neurons can form a two-neuron inertial system by connecting a symmetrical RLC circuit [8], where the output of one neuron is the input of the other. Liao et al. [17,18] considered the dynamical behavior of such neural systems with one delay. They studied the equilibrium stability, Hopf bifurcation and chaotic behavior using the normal form, center manifold, and numerical simulations.

Neural dynamics may be influenced by two independent varying parameters, such as time delay and coupling weight [19]. Thus, considering the combined influences of these varying parameters, certain codimension-2 bifurcations, such as the Hopf-pitchfork bifurcation [20], the double Hopf bifurcation [21], and the Bogdanov-Takens (BT) bifurcation [22,23], were investigated to obtain a global perspective on system dynamics. Recently, He et al. [24] exhibited the global perspective of system dynamics by employing the BT bifurcation in a single delayed inertial neural system. For an inertial two-neuron model with a single delayed coupling, Dong et al. [25] found some stability coexistences for two resting states, two periodic solutions, and two quasi-periodic activities by studying the Hopf-pitchfork bifurcation. Ge and Xu [26] showed the combined effects of coupling weight and time delay on the dynamical behavior of an inertial four-neuron bidirectional associative memory system.

To the best of our knowledge, no research has thus far been conducted on the dynamical analysis of multi-delayed inertial neural systems, and this motivates our present research. In fact, multiple delays should be considered in neural systems (for instance, ref. [21,27,28]). The dynamical investigation of combined multi-delay influences facilitated the development of neural network applications for a few engineering problems. In this paper, we outline a few critical conditions for multiple equilibria and stability switches in inertial neural systems with multiple delays. In particular, one of the codimension-2 bifurcations – the BT bifurcation– is investigated for global dynamics through the normal form system. Although the inertial neural system is similar to the model in [8,9], it involves multiple delays and is established as follows:

$$\begin{cases} \ddot{x}(t) = -a_1\dot{x}(t) - b_1x(t) + c_1f(y(t) - h_2y(t-\tau_2)), \\ \ddot{y}(t) = -a_2\dot{y}(t) - b_2y(t) + c_2f(x(t) - h_1x(t-\tau_1)), \end{cases} \tag{1}$$

where a_i, b_i, c_i>0, and h_i⩾0 are all nonnegative real numbers, $x(t)$ and $y(t)$ denote the activation level of a neuron, whereas c_1 and c_2 correspond to the neuron interaction coefficient. Further, h_1 and h_2 represent the inhibitory influence of neural history. This implies that neuron response is modulated by a dynamical threshold that depends on the history of its activation [29,30]. τ_i>0 (i=1, 2) are coupling delays of inertial neurons that can lead to wide-ranging behaviors in system dynamics. For simplicity, we assume that the activation function is $f(x)$=tanh (x).

Employing the following transformation [29],

$$\begin{cases} z_1(t) = x(t) - h_1x(t-\tau_1), \\ z_2(t) = y(t) - h_2y(t-\tau_2), \end{cases}$$

one obtains the following system which is topologically equivalent to system (1).

$$\begin{cases} \dot{x}_1(t) = x_2(t), \\ \dot{y}_1(t) = y_2(t), \\ \dot{x}_2(t) = -a_1x_2(t) - b_1x_1(t) + c_1f(y_1(t)) - c_1h_1f(y_1(t-\tau_1)), \\ \dot{y}_2(t) = -a_2y_2(t) - b_2y_1(t) + c_2f(x_1(t)) - c_2h_2f(x_1(t-\tau_2)), \end{cases} \tag{2}$$

where $x_1(t) = z_1(t), x_2(t) = \dot{z}_1(t), y_1(t) = z_2(t), y_2(t) = \dot{z}_2(t)$.

The structure of this paper is as follows. In the next section, the number of equilibrium points is theoretically studied and the corresponding pitchfork bifurcation is numerically exhibited. The system model illustrates a single equilibrium, as well as three equilibria for different values of the coupling weights. In section 3, asymptotic stability near the equilibrium point is studied by employing the characteristic equation, and stability conditions involving multiple delays are obtained. The analyses indicate that dynamical stability-switching may occur in some delayed regions. Further, stable regions are shown in the delayed parameter plane using the Hopf bifurcation curve. In order to obtain the global perspective on system dynamics, the stability and periodic activity involved in multiple equilibria are investigated in Section 4 by analyzing the intersection point of the pitchfork and the Hopf bifurcation curves, which is BT bifurcation. The homoclinic bifurcation and the fold bifurcation of the limit cycle are obtained by employing the theoretical results of the third-order BT normal form. Some numerical simulations are used to verify these theoretical results. We conclude with our reflections in Section 5.

2 Equilibrium and pitchfork bifurcation analysis

In this section, we theoretically study the equilibrium point of the system and numerically exhibit the corresponding pitchfork bifurcation. It is obvious that (x_1, y_1, x_2, y_2)=(0, 0, 0, 0) is the trivial point of the system in eq. (2). The linearizing system in eq. (2) near the point (0, 0, 0, 0) produces the following linear system:

$$\begin{cases} \dot{x}_1(t) = x_2(t), \\ \dot{y}_1(t) = y_2(t), \\ \dot{x}_2(t) = -a_1 x_2(t) - b_1 x_1(t) + c_1 y_1(t) - c_1 h_1 y_1(t-\tau_1), \\ \dot{y}_2(t) = -a_2 y_2(t) - b_2 y_1(t) + c_2 x_1(t) - c_2 h_2 x_1(t-\tau_2). \end{cases} \tag{3}$$

The corresponding characteristic equation is

$$\begin{aligned} F(\lambda) = {} & b_1 b_2 - c_1 c_2 + c_1 c_2 h_1 \mathrm{e}^{-\lambda\tau_1} + c_1 c_2 h_2 \mathrm{e}^{-\lambda\tau_2} - c_1 c_2 h_1 h_2 \mathrm{e}^{-\lambda\tau_1 - \lambda\tau_2} \\ & + (a_2 b_1 + a_1 b_2)\lambda + (a_1 a_2 + b_1 + b_2)\lambda^2 + (a_1 + a_2)\lambda^3 + \lambda^4 \\ = {} & 0. \end{aligned} \tag{4}$$

Therefore,

$$F(0) = b_1 b_2 - c_1 c_2 (1-h_1)(1-h_2). \tag{5}$$

Then, if system parameters are $b_1 b_2 < c_1 c_2 (1-h_1)(1-h_2)$, we have $F(\lambda) \to +\infty$, $\lambda \to +\infty$ and $F(0) < 0$ for all values of $\tau_1 \geqslant 0$ and $\tau_2 \geqslant 0$. Further, $F(\lambda)$ is a continuous function with regard to λ. There exist $\lambda^* > 0$ that satisfies $F(\lambda^*) = 0$ for $\tau_1 \geqslant 0$ and $\tau_2 \geqslant 0$. Thus, the characteristic eq. (4) exhibits a zero having the positive real part. The trivial point exhibits delayed independent instability.

To exhibit the varying location of the equilibrium point, static bifurcation is investigated in system (2). This implies that an eigenvalue crosses the imaginary axis for varying system parameters. Assigning λ=0 in (4), we obtain system (2) exhibiting a static bifurcation at (0, 0, 0, 0) if $b_1 b_2 = c_1 c_2 (1-h_1)(1-h_2)$. Because neural system (2) always has the equilibrium point (0, 0, 0, 0), the static bifurcation is either pitchfork bifurcation or transcritical bifurcation. In what follows, employing some theoretical analyses, one exhibits neural system (2) to undergo a pitchfork bifurcation.

The equilibrium point of neural network system (2) satisfies the following equations:

$$\begin{cases} b_1 x_1 = c_1 f(y_1) - c_1 h_1 f(y_1), \\ b_2 y_1 = c_2 f(x_1) - c_2 h_2 f(x_1). \end{cases} \tag{6}$$

From (6), we observe that x_1 satisfies

$$b_1 x_1 + c_1 (h_1 - 1) f\left(c_2 (1-h_2) f(x_1)/b_2\right) = 0. \tag{7}$$

Let $h(x_1) = b_1 x_1 + c_1 (h_1 - 1) f\left(c_2 (1-h_2) f(x_1)/b_2\right)$, then

$$\begin{aligned} h'(x_1) = {} & b_1 - c_1 c_2 (h_1 - 1)(h_2 - 1) f'(x_1) \times \\ & f'\left(c_2 (1-h_2) f(x_1)/b_2\right)/b_2. \end{aligned} \tag{8}$$

Obviously, $h'(0) = b_1 - c_1 c_2 (h_1 - 1)(h_2 - 1)/b_2$.

Supposing $b_1 b_2 > c_1 c_2 (1-h_1)(1-h_2)$, one has $h'(0) > 0$. Further, from $f(u)$=tanh (u), we notice that $f'(u)$ obtains its maximum value if u=0, i.e.,

$$\max_{u \in R} f'(u) = f'(0) = 1. \tag{9}$$

i) If $(1-h_1)(1-h_2) > 0$, then by (8) and (9) we have

$$\begin{aligned} h'(x_1) = {} & b_1 - c_1 c_2 (h_1 - 1)(h_2 - 1) f'(x_1) \times \\ & f'\left(c_2 (1-h_2) f(x_1)/b_2\right)/b_2 \\ \geqslant {} & b_1 - c_1 c_2 (h_1 - 1)(h_2 - 1)/b_2 = h'(0) > 0. \end{aligned}$$

ii) If $(1-h_1)(1-h_2) \leqslant 0$, it is clear that

$$\begin{aligned} h'(x_1) = {} & b_1 - c_1 c_2 (h_1 - 1)(h_2 - 1) f'(x_1) \\ & \times f'\left(c_2 (1-h_2) f(x_1)/b_2\right)/b_2 \geqslant b_1 > 0. \end{aligned}$$

Therefore, $h'(x_1) > 0$ provided $b_1 b_2 > c_1 c_2 (1-h_1)(1-h_2)$ is true; subsequently, $h(x_1)$ is a monotonically increasing function on R. It is obvious that $h(0)$=0. Therefore, $h(x_1)$=0 has the single root x_1=0. This shows that (7) only has a solution at (0, 0, 0, 0).

We now analyze the case where $b_1 b_2 < c_1 c_2 (1-h_1) \times (1-h_2)$. In this case, $h'(0) < 0$, implying that there is a neighborhood $U(0, \varepsilon)$ that is satisfied by $h'(x_1) < 0$ for $x_1 \in U(0, \varepsilon)$. Further, $h(0) = 0$, suggesting that $h(x_1) < 0$ for $x_1 \in U(0, \varepsilon)$ and $x_1 > 0$. Furthermore, employing the neural activation function $|f(u)|=|\tanh(u)| \leqslant 1$, we obtain $h(x_1) \to +\infty$, $x_1 \to +\infty$. Thus, there exists a $x_1^1 > 0$ satisfying $h(x_1^1) = 0$, $h'(x_1^1) \geqslant 0$ and $h(x_1) < 0$ for $x_1 \in (0, x_1^1)$. Considering

$$H(x_1) = h(x_1 + x_1^1) = b_1 (x_1 + x_1^1) + c_1 (h_1 - 1) f(\bar{x}_1^1), \tag{10}$$

where $\bar{x}_1^1 = c_2 (1-h_2) f(x_1 + x_1^1)/b_2$, we can obtain $H(0) = h(x_1^1) = 0$ and

$$H'(x_1) = b_1 - c_1 c_2 (h_1 - 1)(h_2 - 1) f'(x_1 + x_1^1) f'(\bar{x}_1^1)/b_2. \tag{11}$$

It is obvious that $f'(\bar{x}_1^1) \leqslant f'(\bar{x}_1^0)$ is true, when $\bar{x}_1^0 = c_2 (1-h_2) f(x_1^1)/b_2$. Thus, the following conclusion can be obtained for all $x_1 \geqslant x_1^1$,

$$\begin{aligned} H'(x_1) & \geqslant b_1 - c_1 c_2 (h_1 - 1)(h_2 - 1) f'(x_1^1) f'(\bar{x}_1^0)/b_2 \\ & = h'(x_1^1) \geqslant 0. \end{aligned}$$

Thus, the equation $h(x_1) = 0$ only has a solution x_1^1 on $(0, +\infty)$. Let $y_1^1 = \bar{x}_1^1$. Then, (6) has a solution only at $(x_1^1, y_1^1, 0, 0)$, such that $x_1^1 > 0$. Similarly, we observe that equation (6) has only one other root satisfying $x_1^2 < 0$. Therefore, we have the following theorem:

Theorem 1. System (2) displays a pitchfork bifurcation at the point $(0,0,0,0)$ when $b_1 b_2 = c_1 c_2 (1-h_1)(1-h_2)$. To be more precise, the neural system (2) exhibits the single equilibrium point (0,0,0,0) for $b_1 b_2 > c_1 c_2 (1-h_1)(1-h_2)$. Further, there exist three equilibria, one of which is (0,0,0,0) and the other is nontrivial, for $b_1 b_2 < c_1 c_2 (1-h_1)(1-h_2)$.

For example, choosing a_1=0.7, a_2=0.5, b_1=0.9, b_2=1.2, and h_2=0.4, we obtain the pitchfork bifurcation curves illustrated in the (c_1, c_2) plane, in Figure 1(a) for h_1=0.8, and in Figure 1(b) for h_1=1.8. It follows that two bifurcation diagrams are different for thinking the system parameters with positive value. In fact, system (2) undergoes a pitchfork bifurcation under the necessary condition $(1-h_1)(1-h_2)>0$. When h_1=1.8, a bifurcation curve may result for a negative value of c_2 (refer Figure 1(b)). Figure 2 shows one-dimension bifurcation diagrams corresponding to c_1=5 along Line 1 (Figures 2(a) and (b)) and c_2=5 along Line 2 (Figures 2(c) and (d)), respectively. It follows that system (2) exhibits multiple equilibrium points by using the pitchfork bifurcation at the trivial point (0, 0, 0, 0).

3 Stability switches and Hopf bifurcation

In this section, we study the stability of the trivial equilibrium point to find some stability criteria. The necessary and sufficient condition for the point (0, 0, 0, 0) to be asymptotically stable is that all roots of the characteristic eq. (4) have

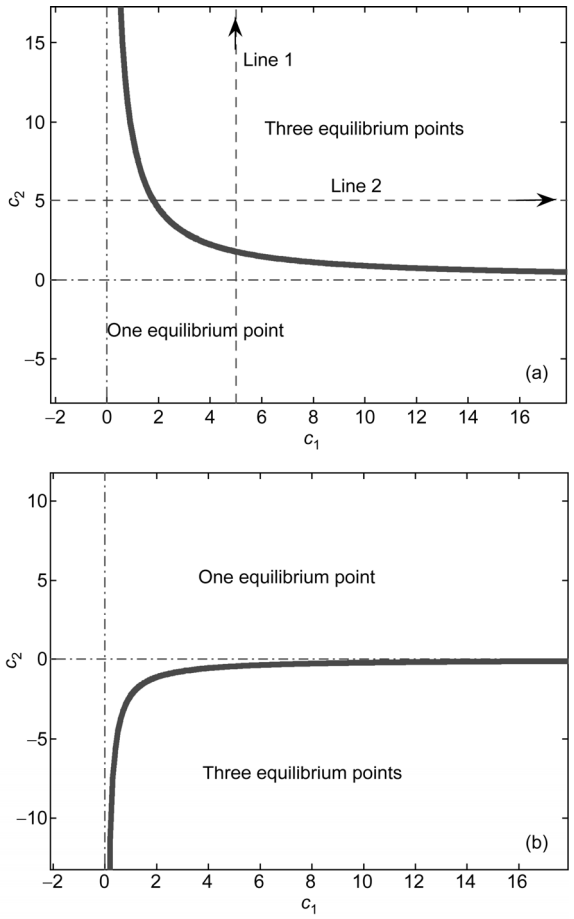

Figure 1 Pitchfork bifurcation curve splits the (c_1, c_2) plane into two regions for (a) h_1=0.8 and (b) h_1=1.8, where the other parameter values are a_1=0.7, a_2=0.5, b_1=0.9, b_2=1.2 and h_2=0.4.

negative real parts. To this end, we begin, for simplicity, with the case where τ_2=0 as follows:

$$b_1b_2 - c_1c_2 + c_1c_2h_2 + c_1c_2h_1e^{-\lambda\tau_1} - c_1c_2h_1h_2e^{-\lambda\tau_1} + (a_2b_1 + a_1b_2)\lambda + (a_1a_2 + b_1 + b_2)\lambda^2 + (a_1 + a_2)\lambda^3 + \lambda^4 = 0. \quad (12)$$

Without loss of generality, letting τ_1=0 in (12) implies

$$\lambda^4 + m_3\lambda^3 + m_2\lambda^2 + m_1\lambda + m_0, \quad (13)$$

where

$$m_3 = a_1 + a_2,\ m_2 = b_1 + b_2 + a_1a_2,\ m_1 = a_1b_2 + a_2b_1,$$
$$m_0 = b_1b_2 - c_1c_2 + c_1c_2h_1 + c_1c_2h_2 - c_1c_2h_1h_2.$$

Employing the Routh-Hurwitz criterion, we obtain the necessary and sufficient condition for all zeros of (13) with the negative real parts:

$$m_3 > 0,\ m_0 > 0,\ m_2m_3 - m_1 > 0,\ m_1m_2m_3 - m_1^2 - m_0m_3^2 > 0. \quad (14)$$

This implies that when system parameters are in accord with conditions expressed in eq. (14), the trivial point has local asymptotic stability for non-delayed systems.

As delay τ_1 varies from zero, the trivial point may tend to instability. To exhibit the critical values, supposing eq. (12) has a pair of pure imaginary roots $\lambda=\pm i\nu(\nu>0)$, we obtain

$$b_1b_2 - c_1c_2 + c_1c_2h_1e^{-i\nu\tau_1} + c_1c_2h_2 - c_1c_2h_1h_2e^{-i\nu\tau_1} + i(a_2b_1 + a_1b_2)\nu - (a_1a_2 + b_1 + b_2)\nu^2 - i(a_1 + a_2)\nu^3 + \nu^4 = 0. \quad (15)$$

Separating (15) into real and imaginary parts provides

$$\begin{cases} b_1b_2 - c_1c_2 + c_1c_2h_2 - (a_1a_2 + b_1 + b_2)\nu^2 + \nu^4 \\ \qquad + c_1c_2h_1(1-h_2)\cos\nu\tau_1 = 0, \\ (a_2b_1 + a_1b_2)\nu - (a_1 + a_2)\nu^3 - c_1c_2h_1(1-h_2)\sin\nu\tau_1 = 0. \end{cases} \quad (16)$$

Eliminating τ_1 from (16) by $\sin^2\nu\tau_1 + \cos^2\nu\tau_1 = 1$, we obtain

$$L_1(\nu) = \nu^8 + n_6\nu^6 + n_4\nu^4 + n_2\nu^2 + n_0 = 0, \quad (17),$$

where

$$n_6 = a_1^2 + a_2^2 - 2(b_1 + b_2),$$
$$n_4 = 4a_1a_2b_1 + 2a_2^2b_1 + b_1^2 + a_1^2(a_2^2 - 2b_2) + 4b_1b_2 + b_2^2 - 2c_1c_2(1-h_2),$$
$$n_2 = a_2^2b_1^2 - 2b_1^2b_2 + b_2(a_1^2b_2 + 2c_1c_2(1-h_2)) - 2a_1a_2(2b_1b_2 - c_1c_2(1-h_2)) - 2b_1(b_2^2 - c_1c_2(1-h_2)),$$
$$n_0 = (b_1b_2 + c_1c_2(1+h_1)(-1+h_2))(b_1b_2 - c_1c_2(1-h_1-h_2+h_1h_2)).$$

Thus, we have the following theorem:

Theorem 2. If neural system (2) has values expressed by eq. (14), the following conclusions hold:

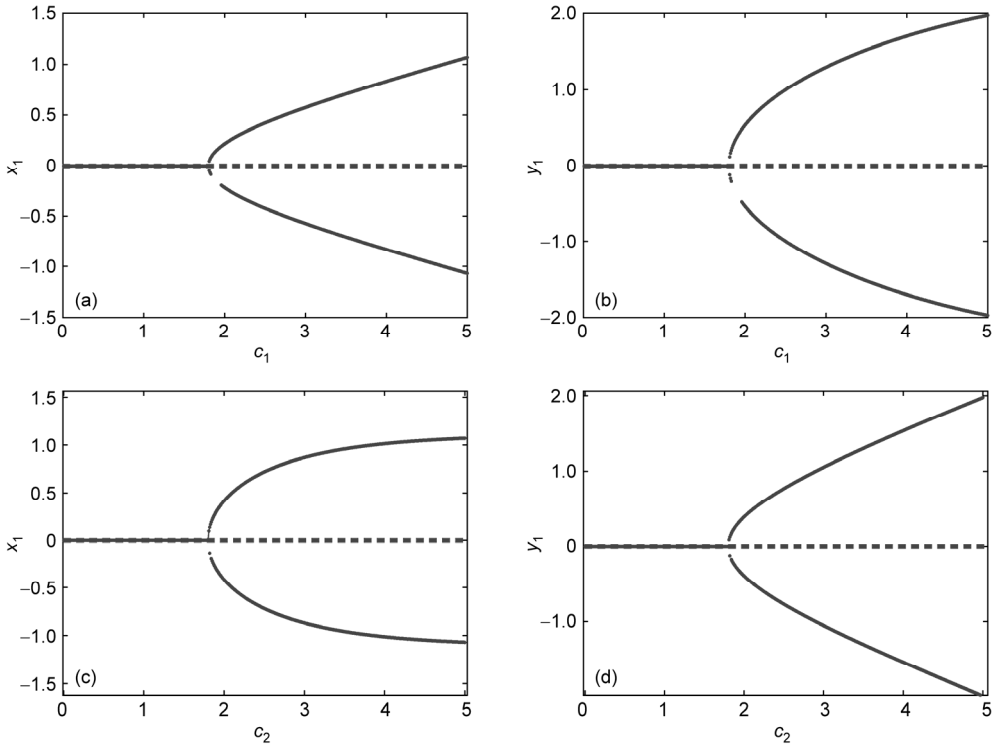

Figure 2 One-dimension bifurcation diagrams corresponding to (a) (c_1, x_1) (b) (c_1, y_1) for the fixed c_2=5 and (c) (c_2, x_1) (d) (c_2, y_1) for c_1=5, where the other parameters are a_1=0.7, a_2=0.5, b_1=0.9, b_2=1.2, h_1=0.8 and h_2=0.4.

(i) When $L_1(v)$=0 does not have the root v>0, all zeros of (12) exhibit negative real parts for any delayed τ_1 values.

(ii) When $L_1(v)$=0 exhibits only a single real root v>0, a critical value $\tau_1^c > 0$ can be obtained, where eq. (12) exhibits all roots with negative real parts for $\tau_1 \in (0, \tau_1^c)$ and the least root with a positive part for $\tau_1 > \tau_1^c$.

(iii) When $L_1(v)$=0 exhibits two least positive real roots $0<v_1<v_2<\cdots$, we can obtain a τ_1-delayed interval sequence for eq. (12) to exhibit all roots with negative real parts.

To obtain the combined effects of multiple delays on system dynamics, we consider delay τ_2 to be the variable parameter for the chosen τ_1. Letting $\lambda=i\omega$ as the simple root of (4), one obtains

$$\begin{aligned} &b_1b_2 - c_1c_2 + c_1c_2\mathrm{e}^{-i\omega\tau_1}h_1 + c_1c_2h_2\mathrm{e}^{-i\omega\tau_2} + i(a_2b_1 + a_1b_2)\omega \\ &-c_1c_2\mathrm{e}^{-i\omega\tau_1}\mathrm{e}^{-i\omega\tau_2}h_1h_2 - (a_1a_2 + b_1 + b_2)\omega^2 - i(a_1 + a_2)\omega^3 + \omega^4 = 0. \end{aligned} \tag{18}$$

Separating the real and imaginary parts provides

$$\begin{cases} b_1b_2 - c_1c_2 - (a_1a_2 + b_1 + b_2)\omega^2 + \omega^4 + c_1c_2h_1\cos\omega\tau_1 \\ \quad + c_1c_2h_2\cos\omega\tau_2 - c_1c_2h_1h_2\cos\omega\tau_1\cos\omega\tau_2 \\ \quad + c_1c_2h_1h_2\sin\omega\tau_1\sin\omega\tau_2 = 0, \\ (a_2b_1 + a_1b_2)\omega - (a_1 + a_2)\omega^3 - c_1c_2h_1\sin\omega\tau_1 \\ \quad + c_1c_2h_1h_2\cos\omega\tau_2\sin\omega\tau_1 - c_1c_2h_2\sin\omega\tau_2 \\ \quad + c_1c_2h_1h_2\cos\omega\tau_1\sin\omega\tau_2 = 0. \end{cases} \tag{19}$$

Eliminating τ_2 from (19), we have

$$\cos\omega\tau_2 = f_1(\omega)/f_3(\omega),\ \ \sin\omega\tau_2 = f_2(\omega)/f_3(\omega), \tag{20}$$

where

$$\begin{aligned} f_1(\omega) &= -b_1b_2 + c_1c_2 + c_1c_2h_1^2 + (a_1a_2 + b_1 + b_2)\omega^2 - \omega^4 \\ &\quad + h_1(b_1b_2 - 2c_1c_2 - (a_1a_2 + b_1 + b_2)\omega^2 + \omega^4)\cos\omega\tau_1 \\ &\quad + h_1\omega(-a_2b_1 - a_1b_2 + (a_1 + a_2)\omega^2)\sin\omega\tau_1, \\ f_2(\omega) &= \omega(-a_2b_1 - a_1b_2 + (a_1 + a_2)\omega^2)(-1 + h_1\cos\omega\tau_1) \\ &\quad + h_1(-b_1b_2 + (a_1a_2 + b_1 + b_2)\omega^2 - \omega^4)\sin\omega\tau_1, \\ f_3(\omega) &= -c_1c_2h_2(1 + h_1^2 - 2h_1\cos\omega\tau_1). \end{aligned}$$

This implies that

$$G(\omega) = f_1^2(\omega) + f_2^2(\omega) - f_3^2(\omega) = 0. \tag{21}$$

If (21) exhibits some positive zeros ω_i, $i = 1, 2, \cdots$, eq. (4) takes the following delayed critical values determined by (20):

$$\tau_{i,j} = (\phi_i + 2j\pi)/\omega_i,\ i = 1, 2, \cdots; j = 0,\ 1,\ 2, \cdots, \tag{22}$$

where $\phi_i \in [0, 2\pi)$ is satisfied by

$$\cos(\phi_i) = f_1(\omega)/f_3(\omega),\ \ \sin(\phi_i) = f_2(\omega)/f_3(\omega).$$

For the sake of simplicity, we represent the minimum value of $\tau_{i,j}$ by τ_c, such that $\tau_c = \min(\tau_{i,j})$. Letting ω_c be

the positive root of (18) for $\tau_2=\tau_c$ and differentiating λ with respect to τ_2 in (4), we obtain

$$\lambda'(\tau_2)=-(c_1c_2(\mathrm{e}^{\lambda\tau_1}-h_1)h_2\lambda)/(-\mathrm{e}^{\lambda(\tau_1+\tau_2)}(a_2b_1+a_1b_2+2(a_1a_2+b_1+b_2)\lambda+3(a_1+a_2)\lambda^2+4\lambda^3)+c_1c_2(\mathrm{e}^{\lambda\tau_2}h_1\tau_1+\mathrm{e}^{\lambda\tau_1}h_2\tau_2-h_1h_2(\tau_1+\tau_2))). \quad (23)$$

Employing the Hopf bifurcation theory for delayed differential equations, we have:

Theorem 3. The following statement is valid if eq. (15) exhibits all zeros with negative real parts:

(i) When $G(\omega)=0$ does not have the positive root, the trivial point of system (2) exhibits asymptotic stability for the arbitrary delay τ_2.

(ii) When $G(\omega)=0$ exhibits one single positive root satisfying $\mathrm{Re}(\lambda'(\tau_2))\neq 0$, the point (0, 0, 0, 0) of system (2) is asymptotically stable for $\tau_2\in[0,\tau_c)$. Further, system (2) displays a Hopf bifurcation from (0, 0, 0, 0) if $\tau_2=\tau_c$.

(iii) When $G(\omega)=0$ exhibits at least two real roots $0<\omega_1<\omega_2<\cdots$ satisfying $\mathrm{Re}(\lambda'(\tau_2))\neq 0$, there is some delayed interval sequence where (0, 0, 0, 0) is asymptotically stable. This implies that the dynamical behavior of system (2) near the point (0, 0, 0, 0) switches from stability to instability, and back again as time delays increase beyond the critical values.

For example, consider system (2) with the fixed parameters a_1=0.7, a_2=0.5, b_1=0.9, b_2=1.2, h_1=0.8, h_2=0.4, c_1=0.8 and c_2=1.2. The coupling delays τ_1 and τ_2 are the variable parameters. The roots of $G(\omega)$ and the real parts of the eigenvalue in (4) are displayed in Figure 3 for delay τ_1. Figure 3(a) shows that the curve determined by $G(\omega)$ does not intersect with $G(\omega)=0$ when $\omega>0$. This implies that $G(\omega)$ has no positive real root. All eigenvalues exhibit negative real parts, as shown in Figure 3(b). The dynamical behavior of system (2) near the point (0, 0, 0, 0) is locally asymptotically stable for all of τ_2.

With the value of τ_1 increasing to one, the $G(\omega)$ curve moves down and crosses the ω-axis. Function $G(\omega)$ has two positive roots, ω_1=0.5354 and ω_2=0.6975, shown in Figure 3(c). It follows from Figure 3(d) that τ_2 has some regions where the system's eigenvalues are negative. The dynamical behavior becomes stable as τ_2 increases in value. Time delays adjust system (2) into a stability region to suppress system vibrations. When the value τ_1 increases to eight, $G(\omega)$ has two pairs of positive roots, as shown in Figure 3(e). However, at the same time, the maximum eigenvalue of (4) for the fixed delay τ_2=0 – that is, the characteristic equation (15) – has a positive real part, as shown in Figure 3(f). System (2) is unstable at the trivial point for all delays τ_2.

The partial eigenvalues and time histories of system (2) with τ_1=1.0 are shown in Figures 4 and 5 for varying delay τ_2. When the time delay is set to τ_2=1.0, the maximum eigenvalue is –0.0204±0.7067i, as shown in Figure 4(a). This implies that the system is locally asymptotically stable at the trivial point, as shown in Figure 5(a). Considering τ_1= 1.0 and varying τ_2, we obtain the maximum eigenvalues in the right-hand plane by crossing the imaginary axis. When τ_2=4.0, the maximum eigenvalues are 0.0391±0.5957i (Figure 4(b)). This implies that the trivial point loses its stability. The temporal history of the system is shown in Figure 5(b). With increase in the delay τ_2, the maximum eigenvalues with negative real parts return to the left-half of the plane. Figure 4(c) illustrates the eigenvalues with –0.0141±0.5232i for τ_2=7.0. The stability of the trivial equilibrium is controlled by delay τ_2, which is shown in Figure 5(c). Further, if τ_2=12.0, the pair eigenvalues have the positive real part 0.0226±0.65i (Figure 4(d)). The trivial point loses its stability, as shown in Figure 5(d). In short, multiple delays induce the dynamic system to exhibit multi-stable regions. The trivial point shows the multiple switching from stability to instability, and back to stability.

Figure 6 shows the global perspective of stability regions illustrated in the (τ_1,τ_2) plane for fixed parameters a_1=0.7, a_2=0.5, b_1=0.9, b_2=1.2, c_1=0.8, c_2=1.2, h_1=0.8 and h_2=0.4. The (τ_1,τ_2) plane is divided into different regions with stable/ unstable trivial equilibrium points. It follows from Figure 6 that the trivial equilibrium is the delay τ_2-independent stability when $\tau_1\in(0, 0.707)$. However, the point exhibits multiple switching from stability to instability and back to stability, if delay τ_1 surpasses its critical value, τ_2=0.707. This circumstance is called delayed dependent stability. Time delays are helpful to control trivial equilibrium.

4 Multi-stability coexistence and BT bifurcation

It follows from section 3 that multiple roots of eq. (21) can lead system (2) near the point (0, 0, 0, 0) to switch between stability and instability when delays surpass the critical values determined by the Hopf bifurcation. Further, system (2) possesses multiple nontrivial equilibrium points using the pitchfork bifurcation. The effects that follow when system (2) employs the Hopf and the pitchfork bifurcations together are described here.

To this end, the Hopf and pitchfork bifurcation curves represented by the coupling weight c_2 and time delay τ_2 are shown in Figure 7. The other parameters are fixed at a_1 = 1.7, a_2=0.5, b_1=0.9, b_2=1.2, c_1=5.0, h_1=0.8, h_2=0.4 and τ_1=0.1. From Theorem 1, system (2) has the critical value for the pitchfork bifurcation, c_2=1.8. To exhibit the type of bifurcation point for the intersection value of the Hopf and pitchfork bifurcation curves, we illustrate the changing trends of ω. In fact, the evolution of ω with coupling weight c_2 is shown in Figure 8. It is obvious that ω approaches zero

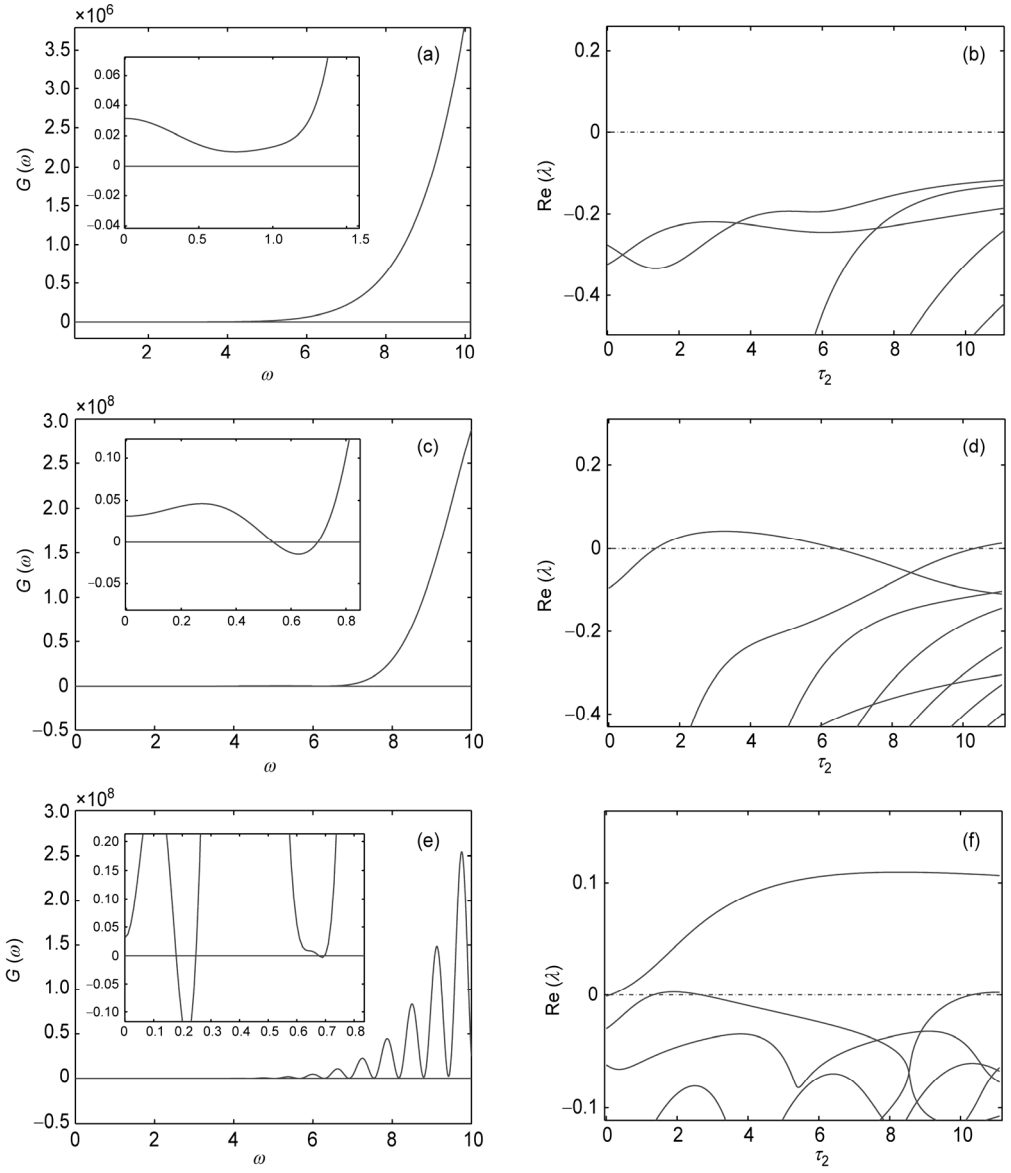

Figure 3 Roots of function $G(\omega)$ (left column) and the real parts of eigenvalues with τ_2 varying (right column) for fixed delays (a)–(b) (τ_1=0), (c)–(d) (τ_1=1.0), and (e)–(f) (τ_1=8.0). The other parameters are a_1=0.7, a_2=0.5, b_1=0.9, b_2=1.2, c_1=0.8, c_2=1.2, h_1=0.8 and h_2=0.4.

when coupling weight c_2 reaches the critical value of the pitchfork bifurcation, 1.8. This suggests that the intersection point is the double zero bifurcation point.

In fact, we can obtain the coordinates of the intersection point using theoretical analysis. It is obvious that eq. (4) has the root λ=0 if

$$b_1 b_2 = c_1 c_2 (1-h_1)(1-h_2) \tag{24}$$

and the derived function of (4) at λ=0 is

$$a_2 b_1 + a_1 b_2 + c_1 c_2 \left(h_1 h_2 \tau_1 + h_1 h_2 \tau_2 - h_1 \tau_1 - h_2 \tau_2\right) = 0. \tag{25}$$

This implies that (4) has a double zero root if conditions (24) and (25) are true. Thus, system (2) assumes a pair-zero eigenvalue for the following critical values:

$$\begin{cases} c_2 = \dfrac{b_1 b_2}{c_1 (1-h_1)(1-h_2)}, \\ \tau_2 = \dfrac{(1-h_2)\left((1-h_1)(a_2 b_1 + a_1 b_2) - b_1 b_2 h_1 \tau_1\right)}{b_1 b_2 (1-h_1) h_2}. \end{cases} \tag{26}$$

The trivial equilibrium point (0, 0, 0, 0) exhibits a codimension-2 singularity, indicating that it has a BT bifurcation.

For example, choosing the system parameters as a_1=1.7, a_2=0.5, b_1=0.9, b_2=1.2, c_1=5.0, h_1=0.8, h_2=0.4 and τ_1=0.1, we obtain the BT bifurcation point (c_2, τ_2)=(1.8, 2.85833), which is the "?" point in Figure 7. The corresponding eigenvalues are shown in Figure 9. System (2) has a zero eigenvalue with multiplicity 2. The trivial equilibrium point

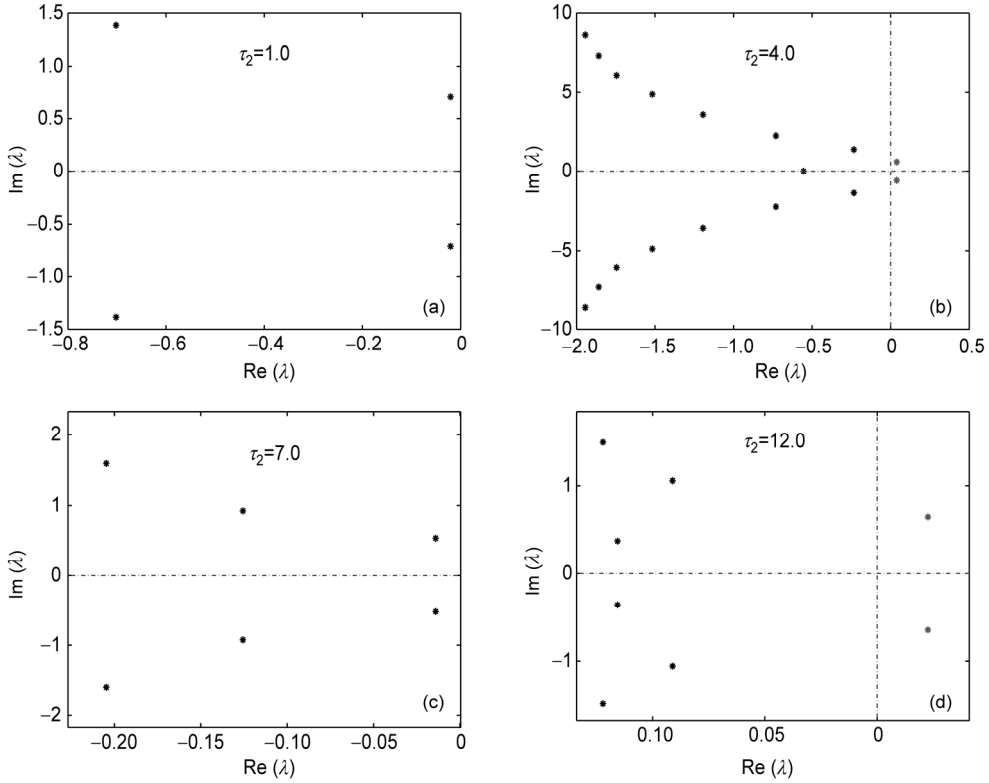

Figure 4 Distribution of partial eigenvalues with delay τ_2 varying as follows: (a) τ_2=1.0, (b) τ_2=4.0, (c) τ_2=7.0, and (d) τ_2=12.0 for fixed parameters a_1=0.7, a_2=0.5, b_1=0.9, b_2=1.2, c_1=0.8, c_2=1.2, h_1=0.8, h_2=0.4 and τ_1=1.0.

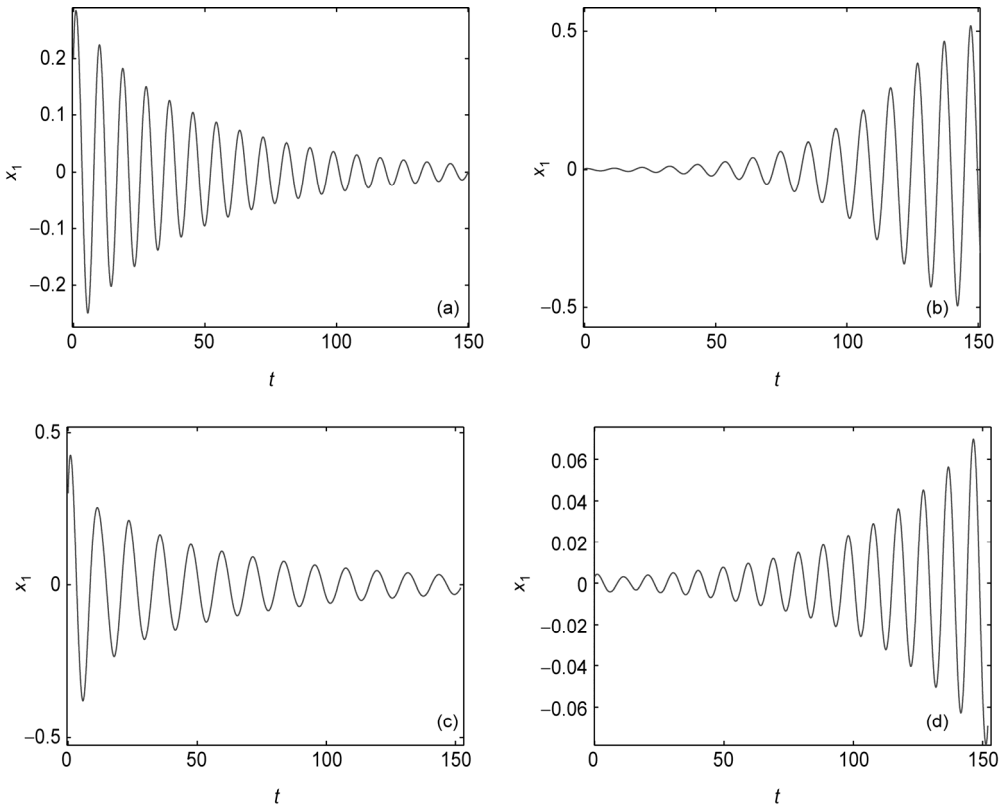

Figure 5 Time histories with delay τ_2 increasing (a) τ_2=1.0, (b) τ_2=4.0, (c) τ_2=7.0, and (d) τ_2=12.0 for fixed parameters a_1=0.7, a_2=0.5, b_1=0.9, b_2=1.2, c_1=0.8, c_2=1.2, h_1=0.8, h_2=0.4 and τ_1=1.0.

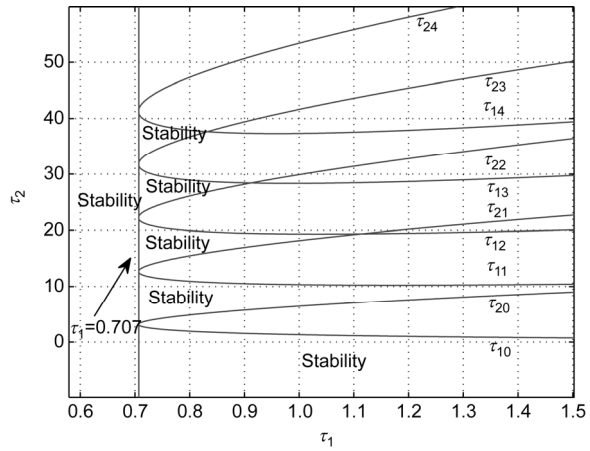

Figure 6 Stability regions in the (τ_1, τ_2) plane for a_1=0.7, a_2=0.5, b_1=0.9, b_2=1.2, c_1=0.8, c_2=1.2, h_1=0.8 and h_2=0.4.

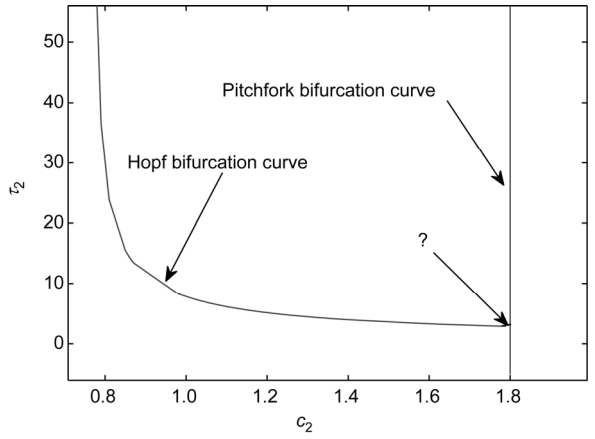

Figure 7 Hopf and pitchfork bifurcation curves in the (c_2, τ_2) plane for parameters a_1=1.7, a_2=0.5, b_1=0.9, b_2=1.2, c_1=5.0, h_1=0.8, h_2=0.4 and τ_1=0.1.

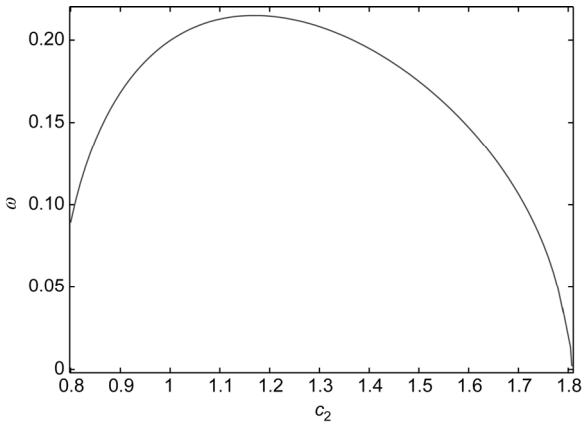

Figure 8 The evolution of ω with coupling weight c_2 for the fixed parameters a_1=1.7, a_2=0.5, b_1=0.9, b_2=1.2, c_1=5.0, h_1=0.8, h_2=0.4 and τ_1=0.1.

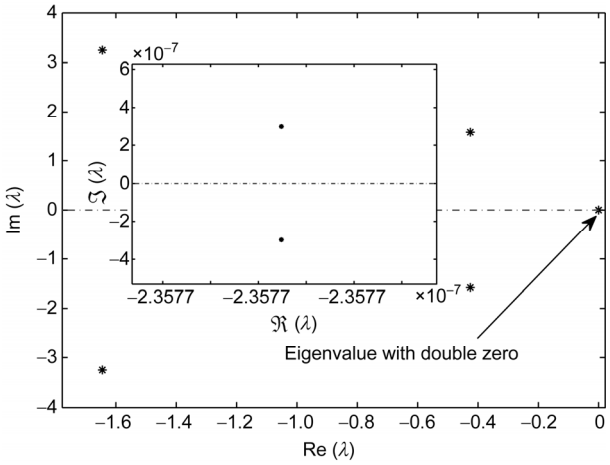

Figure 9 Eigenvalues near the critical value of the BT bifurcation point (c_2, τ_2)=(1.8, 2.85833), where the parameter values are fixed as a_1=1.7, a_2=0.5, b_1=0.9, b_2=1.2, c_1=5.0, h_1=0.8, h_2=0.4, and τ_1=0.1.

exhibits the BT bifurcation.

Considering the activation function of the system $f(x)$= tan h(x) to exhibit $f(-x)=-f(x)$, we obtain system (2) as Z_2-symmetric. The normal form of the BT bifurcation on the center manifold is an odd function, which is topologically equivalent to the dynamic behavior of system (2) near the BT point. Following $f'''(0) = -2 < 0$ and using the computation of the normal form of the function differential equations introduced by [24,32], we can obtain the truncated three-order normal form of the BT bifurcation as follows:

$$\begin{cases} \dot{\eta}_1 = \eta_2, \\ \dot{\eta}_2 = \varepsilon_1\eta_1 + \varepsilon_2\eta_2 - \eta_1^3 - \eta_1^2\eta_2, \end{cases} \tag{27}$$

where ε_1,ε_2 are expressed in terms of the unfolding parameter of time delay τ_2 and coupling weight c_2. Based on nonlinear dynamic theory, complete bifurcation diagrams of system (2) near the BT bifurcation point can be drawn (refer [24,31,32]). Here, we briefly list the results.

Theorem 4. The trivial point of system (2) exhibits a BT bifurcation for conditions (26). The complete bifurcation diagram is obtained as follows:

(i) The system exhibits a pitchfork bifurcation at the trivial point when $F^{(1)} = \{(\varepsilon_1, \varepsilon_2) : \varepsilon_1 = 0, \varepsilon_2 \in R\}$.

(ii) The system exhibits a Hopf bifurcation at the trivial point when $H^{(1)} = \{(\varepsilon_1, \varepsilon_2) : \varepsilon_2 = 0, \varepsilon_1 < 0\}$.

(iii) The system exhibits a Hopf bifurcation at nontrivial points when $H^{(2)} = \{(\varepsilon_1, \varepsilon_2) : \varepsilon_2 = \varepsilon_1, \varepsilon_1 > 0\}$.

(iv) The system exhibits a homoclinic bifurcation when $P = \{(\varepsilon_1, \varepsilon_2) : \varepsilon_2 = 4/5 \times \varepsilon_1 + o(\varepsilon_1), \varepsilon_1 > 0\}$.

(v) The system exhibits a fold bifurcation of the limit cycle when $K = \{(\varepsilon_1, \varepsilon_2) : \varepsilon_2 = \kappa_0\varepsilon_1 + o(\varepsilon_1), \varepsilon_1 > 0, \kappa_0 = 0.752\cdots\}$.

The phase portraits and bifurcation diagram are shown in Figure 10. Using these bifurcation curves, the parameter (τ_2,

c_2) plane is divided into different dynamical regions. The numerical simulations of the phase portraits near the BT bifurcation point are shown in Figure 11.

In region 1 of Figure 10, the dynamic system has a unique trivial equilibrium with the stability. The phase portrait by numerical simulation is shown in Figure 11(a). The stable point then exhibits a non-degenerate Hopf bifurcation on the left half-axis $H^{(1)}$, resulting in a stable periodic motion shown in Figure 11(b).

Two unstable nodes branch from the trivial point if the system parameters pass through the upper half-line of $F^{(1)}$ from region 2 to 3. In region 3, three equilibrium points are located in the "big" periodic motion generated in region 2, as shown in Figure 11(c).

In region 4, there exist three periodic motions, a "big" stable one and two "small" unstable ones (refer Figure 11(d)). In fact, at the curve of $H^{(2)}$, the nontrivial equilibrium points simultaneously exhibit Hopf bifurcations. This leads to the generation of two "small" unstable periodic motions around the nontrivial equilibrium points. The dynamical behavior near the nontrivial equilibrium points becomes stable.

Unfortunately, the unstable limit cycle cannot be displayed by numerical simulation in the delayed dynamical system. However, the phase portrait of region 4 is different from the one for region 5. The blank spaces around the nontrivial equilibria shown in Figure 11(d) are located the unstable limit cycles, which disappear in region 5.

Traversing line P from region 4 to 5 corresponds to the disappearance of "small" periodic motions and the generation of another unstable "big" periodic motion. At this point, the "small" motions around the nontrivial equilibria in region 4 disappear on account of a homoclinic bifurcation with a symmetric figure-8 shape. The saddle trivial equilibrium has two simultaneous homoclinic orbits. The "big" stable limit cycle and the two stable nontrivial equilibrium points are shown in Figure 11(e).

Finally, the two "big" periodic motions collide with and destroy each other when they cross the line K, called the fold bifurcation of the limit cycle. Through such fold bifurcations, no periodic motions persist in the neural system. Therefore, we have three equilibrium points in region 6, the trivial saddle point and two stable symmetry-coupled nontrivial foci/nodes (refer Figure 11(f)). The nontrivial equilibrium points both collide with the trivial point at the lower half-line $F^{(2)}$, as the function returns to region 1.

5 Conclusions

Time delays are a crucial factor in signal transmission between biological neurons or electronically modeled neurons. Multiple delays induce neural systems to exhibit richer dynamical behaviors. In this paper, we studied an inertial two-neuron coupling model with multiple delays. We analyze the number of equilibrium points and exhibit the corresponding pitchfork bifurcation. The system has a unique equilibrium and three equilibria for different coupling weights. Further, multiple delays greatly complicate the stability regions. The neural system (2) illustrates stability regions on account of delayed dependence and independence. The dynamical system exhibits multiple switching from stability to instability and back to stability as the delay increases. To obtain these thresholds to illustrating stable regions, the Hopf bifurcation curve is shown by employing

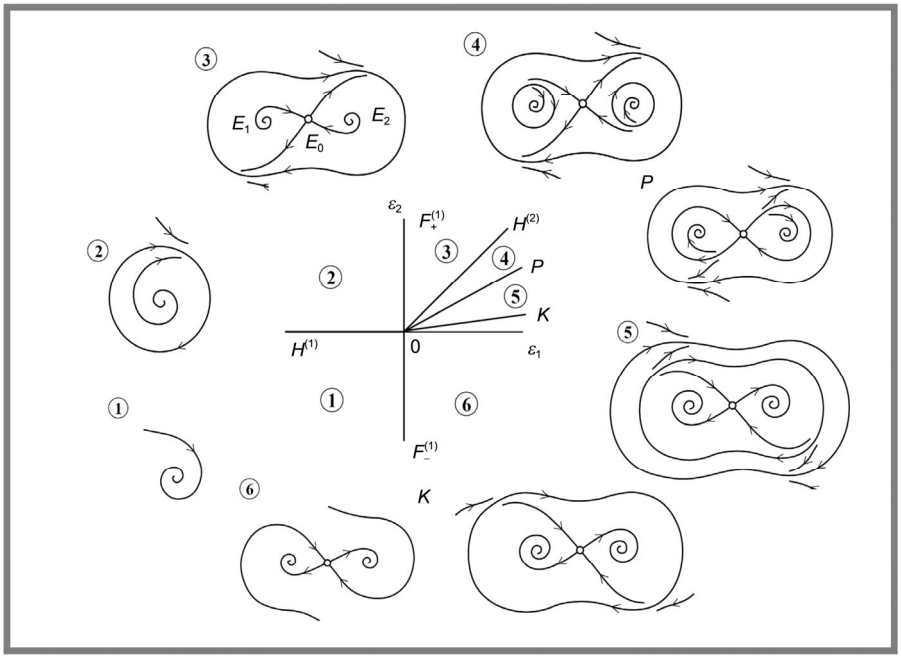

Figure 10 Bifurcation diagram near the critical value of BT bifurcation point [31].

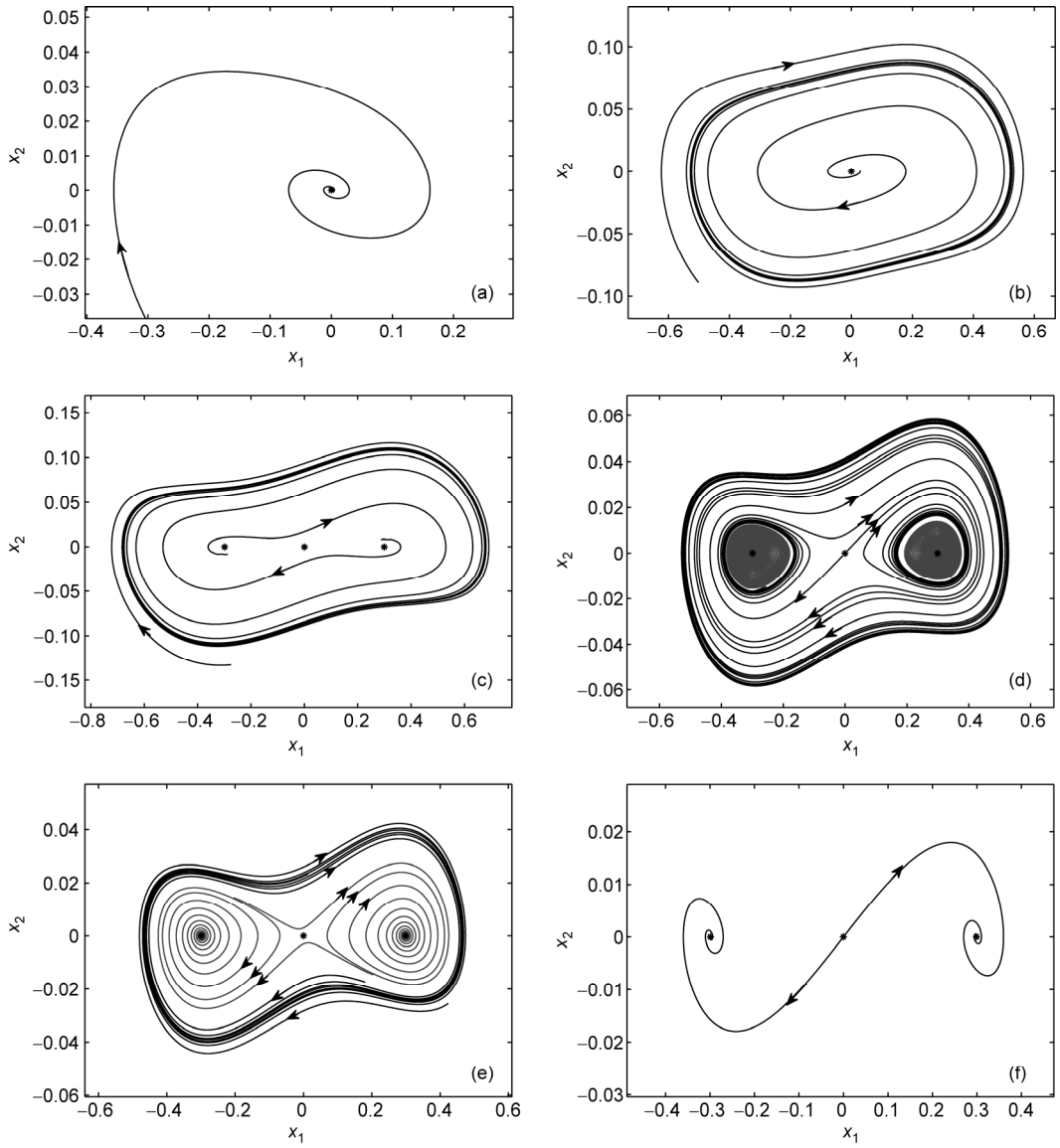

Figure 11 Numerical simulation for phase portraits of neural system (2) near the critical value of BT bifurcation point.

the characteristic equation. The stable region for the trivial equilibrium point is derived in the delayed parameter plane.

The multi-stability of a dynamical system implies the coexistence of multiple steady states for fixed parameter values, which is an important characteristic for engineering applications of neural systems. The long-term dynamic behavior of such systems is extremely sensitive to initial conditions and stochastic disturbances. In order to study the multi-stability of neural systems, we investigated the Bogdanov-Takens bifurcation, obtained by analyzing the natural frequency evolution near the intersection point of the pitchfork and the Hopf bifurcation curves. It was shown that multiple stability coexistence involves two stable equilibrium points as well as the coexistence of two points and one limit cycle by employing the pitchfork bifurcation, the symmetric figure-8 homoclinic bifurcation, and the fold bifurcation of the limit cycle. Further, numerical simulations verify our theoretical results.

This work was supported by the National Natural Science Foundation of China (Grant No. 11302126), the State Key Program of National Natural Science of China (Grant No. 11032009), the Shanghai Leading Academic Discipline Project (Grant No. B302), and Young Teacher Training Program of Colleges and Universities in Shanghai (Grant No. ZZhy12030).

1 Hopfield J J. Neurons with graded response have collective computational properties like those of two-state neurons. Proc Natl Acad Sci (USA), 1984, 81: 3088–3092
2 Schieve W C, Bulsara A R, Davis G M. Single effective neuron. Phys Rev A, 1991, 43: 2613–2623
3 Song Z G, Xu J. Bursting near Bautin bifurcation in a neural network with delay coupling. Int J Neural Syst, 2009, 19: 359–373
4 Song Z G, Xu J. Codimension-two bursting analysis in the delayed neural system with external stimulations. Nonlinear Dyn, 2012, 67: 309–328
5 Ashmore J F, Attwell D. Models for electrical tuning in hair cells.

Proc Royal Soc London B, 1985, 226: 325–334
6 Angelaki D E, Correia M J. Models of membrane resonance in pigeon semicircular canal type II hair cells. Biol Cybernet, 1991, 65: 1–10
7 Mauro A, Conti F, Dodge F, et al. Subthreshold behavior and phenomenological impedance of the squid giant axon. J General Physiol, 1970, 55: 497–523
8 Badcock K L, Westervelt R M. Dynamics of simple electronic neural networks. Physical D, 1987, 28: 305-316
9 Wheeler D W, Schieve W C. Stability and chaos in an inertial two-neuron system. Physical D, 1997, 105: 267-284
10 Tani J, Fujita M. Coupling of memory search and mental rotation by a nonequilibrium dynamics neural network. IEICF Trans Fund Electron Commun Comput Sci E, 1992, 75-A(5): 578–585
11 Tani J. Proposal of chaotic steepest descent method for neural networks and analysis of their dynamics. Electron Commun Jpn, 1992, 75(4): 62–70
12 Campbell S A. Time delays in neural systems. In: McIntosh A R, Jirsa V K, eds. Handbook of Brain Connectivity. Springer, 2007, 65–90
13 Song Z G, Xu J. Bifurcation and chaos analysis for a delayed two-neural network with a variation slope ratio in the activation function. Int J Bifurcat Chaos, 2012, 22: 1250105
14 Liu Q, Liao X F, Yang D G, et al. The research for Hopf bifurcation in a single inertial neuron model with external forcing. In: Lin T Y, Hu X, Han J, et al, eds. IEEE Proceeding of International Conference on Granular Computing, San Jose, California, 2007. 528-533
15 Li C G, Chen G R, Liao X F, et al. Hopf bifurcation and chaos in a single inertial neuron model with time delays. Eur Phys J B, 2004, 41: 337–343
16 Liu Q, Liao X F, Guo S T, et al. Stability of bifurcating periodic solutions for a single delayed inertial neuron model under periodic excitation. Nonlinear Anal-Real World Appl, 2009, 10: 2384–2395
17 Liu Q, Liao X F, Wang G Y, et al. Research for Hopf bifurcation of an inertial two-neuron system with time delay. In: Zhang Y Q, Lin T Y, eds. IEEE Proceeding of International Conference on Granular Computing, Atlanta, USA, 2006. 420–423
18 Liu Q, Liao X F, Liu Y, et al. Dynamics of an inertial two-neuron system with time delay. Nonlinear Dyn, 2009, 58: 573–609
19 Song Z G, Xu J. Stability switches and multistability coexistence in a delay-coupled neural oscillators system. J Theor Biol, 2012, 313(21): 98–114
20 Zhen B, Xu J. Fold–Hopf bifurcation analysis for a coupled Fitz-Hugh-Nagumo neural system with time delay. Int J Bifurcation Chaos, 2010, 20: 3919–3934
21 Song Z G, Xu J. Stability switches and double Hopf bifurcation in a two-neural network system with multiple delays. Cogn Neurodyn, 2013, 7: 505–521
22 Jiang W, Yuan Y. Bogdanov–Takens singularity in Van der Pol's oscillator with delayed feedback. Physica D, 2007, 227: 149–161
23 Jiang J, Song Y. Bogdanov–Takens bifurcation in an oscillator with negative damping and delayed position feedback. Appl Math Modell, 2013, 37: 8091–8105
24 He X, Li C, Shu Y. Bogdanov–Takens bifurcation in a single inertial neuron model with delay. Neurocomputing, 2012, 89: 193–201
25 Dong T, Liao X F, Huang T W, et al. Hopf–pitchfork bifurcation in an inertial two-neuron system with time delay. Neurocomputing, 2012, 97: 223–232
26 Ge J H, Xu J. Weak resonant double Hopf bifurcations in an inertial four-neuron model with time delay. Int J Neural Syst, 2012, 22(1): 63–75
27 Xu X. Local and global Hopf bifurcation in a two-neuron network with multiple delays. Int J Bifurcation Chaos, 2008, 18(4): 1015–1028
28 Campbell S A, Ncube I, Wu J. Multistability and stable asynchronous periodic oscillations in a multiple-delayed neural system. Physica D, 2006, 214(2):101–119
29 Liao X F, Wong K-W, Wu Z F. Asymptotic stability criteria for a two-neuron network with different time delays. IEEE Trans. Neural Networks, 2003, 14(1): 222–227
30 Gopalsamy K, Leung Issic K C. Convergence under dynamical thresholds with delays. IEEE Trans. Neural Networks, 1997, 8(2): 341–348
31 Kuznetsov Y A. Elements of Applied Bifurcation Theory. Springer, New York, 1995
32 Dong T, Liao X. Bogdanov-Takens bifurcation in a tri-neuron BAM neural network model with multiple delays. Nonlinear Dyn, 2013, 71: 583–595